Tumble Kinematics of Escherichia coli near a Solid Surface

Laurence Lemelle, Thomas Cajgfinger, Cao Cuong Nguyen, Agnès Dominjon, Christophe Place, Elodie Chatre, Rémi Barbier, Jean-François Palierne, Cédric Vaillant

Tumble Kinematics of Escherichia coli near a Solid Surface

Laurence Lemelle, Thomas Cajgfinger, Cao Cuong Nguyen, Agnès Dominjon, Christophe Place, Elodie Chatre, Rémi Barbier, Jean-François Palierne, Cédric Vaillant

Please cite this article in press as: Lemelle et al., Tumble Kinematics of *Escherichia coli* near a Solid Surface, Biophysical Journal (2020), https://doi.org/10.1016/j.bpj.2020.03.024

Biophysical *Journal*

Biophysical Society

Tumble Kinematics of *Escherichia coli* near a Solid Surface

Laurence Lemelle,[1,*] Thomas Cajgfinger,[2] Cao Cuong Nguyen,[1] Agnès Dominjon,[2] Christophe Place,[3] Elodie Chatre,[1] Rémi Barbier,[2] Jean-François Palierne,[3] and Cédric Vaillant[3]

[1]Laboratoire de Géologie de Lyon-Terre Planètes et Environnement, ENS de Lyon, Université Claude Bernard, CNRS, Université Lyon, Lyon, France; [2]Institut de Physique des 2 Infinis de Lyon, Institut de Physique des 2 Infinis de Lyon, Université Lyon, Université Claude Bernard, CNRS, Lyon, France; and [3]Laboratoire de Physique, ENS de Lyon, CNRS, Université Lyon, Lyon, France

ABSTRACT Bacteria tumble periodically, following environmental cues. Whether they can tumble near a solid surface is a basic issue for the inception of infection or mineral biofouling. Observing freely swimming *Escherichia coli* near and parallel to a glass surface imaged at high magnification (×100) and high temporal resolution (500 Hz), we identified tumbles as events starting (or finishing, respectively) in abrupt deceleration (or reacceleration, respectively) of the body motion. Selected events show an equiprobable clockwise (CW) or counterclockwise change in direction that is superimposed on a surface CW path because of persistent propulsion. These tumbles follow a common long (about 300 ± 100 ms, $N = 52$) deceleration-reorientation-acceleration pattern. A wavelet transform multiscale analysis shows these tumbles cause in-plane diffusive reorientations with 1.5 rad^2/s rotational diffusivity, a value that compares with that measured in bulk tumbles. In half of the cases, additional few-millisecond bursts of an almost equiprobable CW or counterclockwise change of direction (12 ± 90°, $N = 89$) occur within the reorientation stage. The highly dispersed absolute values of change of direction (70 ± 66°, $N = 89$) of only a few bursts destabilize the cell-swimming direction. These first observations of surface tumbles set a foundation for statistical models of run-and-tumble surface motion different from that in bulk and lend support for chemotaxis near solid surface.

INTRODUCTION

Suspended swimming *Escherichia coli* explore their surroundings by performing a run-and-tumble motion, alternating phases of straight propulsion—the runs—with shorter phases of erratic reorientation—the tumbles—resulting in a random walk. Modulating the run length (1) or the tumbles' directional persistence (2) enables *E. coli* to bias the motion toward preferential conditions or away from detrimental ones. Tumbles are characterized by the disentanglement of a single micrometers-long filament from the propulsive flagellar bundle formed by coalesced rotating filaments (3,4). The bulk random-walk-like motion drastically changes when reaching a solid surface, for instance, at the beginning of a cell infection or of mineral biofouling. Swimming *E. coli* then tend to circle (5,6). Their speed and trajectory radius decrease as they come closer to the surface (7), following the predictions of low-Reynolds hydrodynamics (8,9). Owing to their enhanced near-surface concentration, compared with that in the bulk (10), and to the long residence time they spend swimming parallel to the surface (11,12), swimming *E. coli* are deemed to be trapped on the surface, a feature explained by near-field hydrodynamic coupling between the cell body and the surface during a collision (13).

Although reorientations related to tumbles near a surface (5), whether they were associated with a collision or not, were reported from the first three-dimensional (3D) tracking, little attention has been paid to them. Tumbles were proposed as a possible mechanism whereby trapped bacteria are set free from the surface, thus explaining the shorter surface residence time of the wild-type swimmers compared with the smooth-type swimmers (11). Conversely, the decrease of the switching rate of the bacterial motor under high load (14) and the reduction of the tumble rate in a population within several tens of micrometers from a solid surface (15) suggest that tumbles may be hindered near a solid surface. *E. coli* does not scatter in the same way when swimming beyond 2 μm, a cell length away from a surface (15), or closer, where the hydrodynamic effects are sizeable (12). Whether the close surface proximity

Submitted December 31, 2019, and accepted for publication March 23, 2020.

*Correspondence: laurence.lemelle@ens-lyon.fr

Jean-François Palierne and Cédric Vaillant contributed equally to this work.

Editor: Julie Biteen.

https://doi.org/10.1016/j.bpj.2020.03.024

Please cite this article in press as: Lemelle et al., Tumble Kinematics of *Escherichia coli* near a Solid Surface, Biophysical Journal (2020), https://doi.org/10.1016/j.bpj.2020.03.024

modifies the tumbling frequency and its progress and thereby alters *E. coli*'s ability to orient near a solid surface is still an open question. As in the bulk, three main types of analyzes can be carried out to better understand the tumbling kinematics of *E. coli*: 1) cell body kinematics during tumbling, 2) tumbling frequency, and 3) flagellar dynamics. An experimental study of the cell body kinematics of tumble on a solid surface is presented here.

We study the bacteria tumbles of the swimming wild-type *E. coli* near a glass surface using dark-field video-microscopy at high magnification (×100) and high temporal resolution (500 fps). Such imaging has already proved efficient in following the cell body and the associated flagellum dynamics within bulk tumbles of a uniflagellated bacterium (16). This label-free noninvasive imaging is especially convenient for long-duration imaging. The high aperture and magnification set a shallow focus depth guaranteeing the sampling of trajectories less than a cell length away from the wall, where hydrodynamics is prominent (12). Through image analysis, we determined the speed V and the direction angle Φ of the trajectory of the body centroid (Fig. 1). The tumbles were then extracted as a function of speed drop. Indeed, speed drop, whether abrupt or extended, has been reported to be associated with tumble reorientation (1). Few detection methods using threshold values for speed have been developed and applied in the bulk (17). However, near surfaces, hydrodynamic interaction with the surface causes the speed to decrease, jeopardizing the sensitivity of these methods. The high temporal resolution applied in this study allowed the detection of tumbles not only as long but abrupt drops in speed and to resolve the variations of the track's orientation at different timescales.

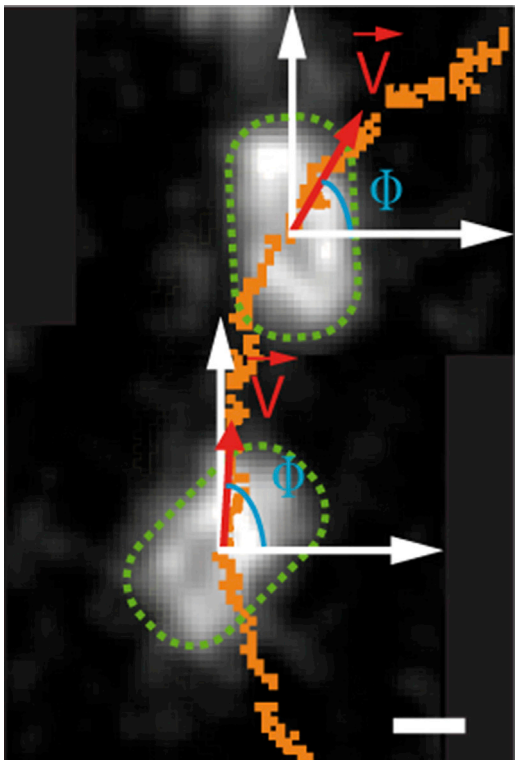

FIGURE 1 High-speed dark-field video microscopy of the *E. coli* body along its trajectory. Orange dots indicate the centroids at 500 fps. The uncertainty is less than the pixel size. Two grayscale intensity images of the body are shown on this trajectory. The contour of the body (in *green dashed line*), the laboratory reference frame (in *white*), the bacterium velocity V (in *red*), and the orientation of the trajectory Φ relative to the x axis (in *blue*) are reported on each image. Scale bars, 1 μm. To see this figure in color, go online.

Preference was given to a closer inspection of a restricted number of tumbles from well-characterized swimming trajectories and a population of a given age and tumbling frequency instead of a large number of events from trajectories alternating between a variety of behaviors (shocks, reversible and irreversible adsorption, tethering) from conditions difficult to compare. The following several properties of tumbles near a solid surface were observed, most notably

1. all tumbles were associated with a drop in velocity, as already observed in the bulk (1), with or without an overall change in orientation;
2. a deceleration phase preceded the reorientation phase, and the average duration of the reorientation was comparable with that reported for motion in the bulk (1);
3. the curvature that prevailed during the surface runs was still active during tumbles, superimposed to a zero-mean random change;
4. two different reorientation mechanisms operated: an ever-present diffusion process with $D = 1.5\ \mathrm{rad}^2 \cdot \mathrm{s}^{-1}$, already found in the bulk (18), together with few or no reorientation bursts.

We discuss how the proximity of the surface may cause bursts.

MATERIALS AND METHODS

Preparing the bacteria

E. coli strain AW474, wild-type, which has been tested for motility and chemotaxis and is resistant to streptomycin, was used for this experimentation. Colonies of *E. coli* were obtained by plating frozen bacteria on a tryptone agar plate (10 g/L tryptone (Difco Laboratories), 8 g/L NaCl (Merck, Darmstadt, Germany), 15 g/L agar (Becton Dickinson, Franklin Lakes, New Jersey)) supplemented with 25 μg/mL streptomycin (Sigma-Aldrich, St. Louis, MO) incubated overnight at 37°C. Isolated colonies were inoculated in a sterile polypropylene tube in 2 mL of tryptone broth (TN) (4 g/L tryptone (Difco Laboratories, Franklin Lakes, New Jersey), 2.5 g/L NaCl (Merck), and 0.4% glycerol (Promega, Madison, WI)). These *E. coli* precultures were grown overnight at 32°C under 300 rpm gyration using a ThermoMixer (Eppendorf, Hamburg, Germany). After one night, bacteria were diluted into 2 mL of fresh TN to an optical density at 600 nm of 0.05 and grown at 32°C and 300 rpm for 3 h and 40 min to reach the exponential phase. The suspension of bacteria grown for 3 h and 40 min until an optical density at 600 nm of 0.340 was diluted twice with TN heated at 32°C. 32 μL of bacteria suspension was sealed within a 100-μm-thin spacer between a coverslip and a microscope slide, carefully avoiding air bubbles.

Please cite this article in press as: Lemelle et al., Tumble Kinematics of *Escherichia coli* near a Solid Surface, Biophysical Journal (2020), https://doi.org/10.1016/j.bpj.2020.03.024

Imaging the bacteria

Dark-field imaging was performed with a DMIRBE Leica inverse microscope equipped with a 100× oil objective (HCX PL APO NA 1.4–0.7; Leica, Wetzlar, Germany) and the oil Cytoviva condenser (NA1.2–1.4; CytoViva, Auburn, AL). Illumination was provided by a 12 V, 0.6 W light (Sunon, Brea, CA) used at minimal intensity. The nonfluorescent contrast red filter from the Cytoviva system was put on the optical path to cut wavelengths of <530 nm that impair bacteria's motility. Images were acquired using an electron-bombarded-CMOS (ebCMOS) camera of single photon sensitivity (Lusipher; Institut de Physique Nucléaire de Lyon, Lyon, France). Its sensor is a 400 × 400 pixel matrix of CMOS 10-μm pitch pixels; its sensitivity is such that a single bombarded electron generates a 5 × 5 pixel cluster with a 40-ADC-units mean intensity per cluster and a one-ADC-unit mean readout noise per pixel. Intensity images encoded on eight bits were captured at 500 fps in 60-s sequences and converted to TIF stacks. Data were transferred with 100% duty cycle and no dead time.

Acquisition of trajectories

Images were analyzed off-line after a Gaussian blurring (5 × 5 pixels). Sets of pixels showing a signal/noise ratio higher than 10 were contoured and interpreted as a bacterium if the pixel area was higher than 200 pixels and the photon number was higher than 100.

Bacteria were located within video frames, and their positions were connected throughout successive frames, thus generating trajectories $x(t)$, $y(t)$. The coordinates of the centroid, x and y, targeted bacterium image of p pixels in the frame were calculated as follows:

$$x = \frac{1}{p}\sum_{k=1}^{k=p} x_k, y = \frac{1}{p}\sum_{k=1}^{k=p} y_k, \tag{1}$$

where x_k and y_k are the coordinates of the k^{th}-pixel of the considered target. A total set of 213 trajectories were reconstructed from the selected swimming experiment. The 150 trajectories that lasted at least 1 s (about one run duration) and that moved by more than 1 μm were selected to search for tumble events.

The dispersion of the position (or orientation, respectively) was evaluated as the standard deviation of the position (or orientation, respectively) distribution of motionless bacteria recorded for 1 s (500 frames); its value, averaged over 50 bacteria, was 25 nm (1.5°, respectively). The coordinates $x(t)$, $y(t)$ were smoothed using a flat sliding window with a width of 50 ms (25 frames). From these quantities, we computed the following speed:

$$V = \sqrt{\dot{x}^2 + \dot{y}^2}, \tag{2}$$

and the trajectory's direction angle,

$$\Phi = \arctan(\dot{y} / \dot{x}). \tag{3}$$

Here and in the following, the overdot denotes a time derivative, e.g., $\dot{x} = \mathrm{d}x = \mathrm{d}t$, numerically approximated by the first difference $\dot{x}_i = (x_{I+1} - x_i)/\Delta t$, where $\Delta t = 2$ ms is the time step.

Sorting tumbles by analyzing the trajectories at coarse-grained scale

Focusing on drops in velocity, we retained tumble events when both the initial speed deceleration was abrupt, and the decrease of speed was significant by testing the following conditions at the deceleration phase:

$$\ddot{V}\left(t_1^V\right) < -\beta, \tag{4}$$

$$V\left(t_1^V\right) - V\left(t_2^V\right) > \alpha V^{mod}, \tag{5}$$

where α and β are threshold values; V^{mod} is the trajectory's modal speed value; and times t_1^V, t_2^V, and t_3^V correspond to the first minimum, maximum, and second minimum, respectively, of the second time derivative of the velocity, $\ddot{V}$. The speed V appearing in Eqs. 2 and 5 and obtained from position coordinates x and y was averaged over 50 ms, and subsequent derivatives with respect to time were taken after drastically reducing the imprinted body wobbling by applying a constant symmetric sliding window with a width of $L = 114$ ms.

Sorting was done by fixing $a = 12\%$ and $\beta = 250$ μm/s^3. The modal and skewness values of the V distribution of each trajectory were compiled to select the trajectories mainly composed of run-tumble-run sequences. A restricted set of 36 trajectories displaying a high-speed modal value together with an asymmetry (skewness < -0.2) toward the lower values, i.e., drops, was sorted.

A total of 52 tumbles were detected for a 58-s total duration of the trajectories. We addressed the sensitivity of this sorting by checking that a constant number of events (± 3) were found for data smoothed at $L = 114$ ms and $L = 50$ ms. The start of the 52 deceleration events t_1^V was detected 6 ms ($\pm$ 20 ms, $N = 52$) earlier for the smoothing scale of $L = 114$ ms than for the smoothing scale of $L = 50$ ms. The resulting enlargement was by 8 ms ($\pm$ 23 ms, $N = 52$), for example, for the period of speed decay, and the relative speed variation was overestimated by 5 $\pm$ 15%.

Directional autocorrelation function

We introduce the tumble direction increment over duration τ of the centered reorientation angle $\Psi(t)$,

$$\delta_\tau \Psi = \Phi(t+\tau) - \Phi(t) - \tau\dot{\Phi}^{mod}, \tag{6}$$

where $\dot{\Phi}^{mod}$ is the modal angular velocity computed in the two adjacent surface runs. We compute the directional autocorrelation function between times t_1 and t_2 as follows:

$$\langle \cos\delta_\tau \Psi \rangle = 1 \Big/ n\sum_{i=0}^{n-1} \cos\left(\Phi(t_i+\tau) - \Phi(t_i) - \dot{\Phi}^{mod}\tau\right), \tag{7}$$

where $n = (t_2 - t_1 - \tau)/\delta t$ and the sum runs over the n possible values of I such that times t_i and $t_i + \tau$ satisfy $t_1 \le t_i < t_i + \tau \le t_2$.

Wavelet analysis of the direction fluctuations

To characterize the stochastic process that controls the reorientation dynamics of the bacteria during tumbles, we performed a multiscale analysis of the centered reorientation $\Psi(t)$ profiles using the wavelet transform (WT) analysis framework (19). Using the first derivative of the Gaussian as the mother wavelet $g^{(1)}(t) = (d/dt)e^{-t^2/2}$, the wavelet transform of the signal $\Psi(t)$ was defined by the following convolution:

$$W_{g^{(1)}}[\Psi](t,\tau) = \frac{1}{\tau}\int_{-\infty}^{+\infty} g^{(1)}\left(\frac{u-t}{\tau}\right)\Psi(u)du. \tag{8}$$

$W_{g^{(1)}}[\Psi](t,\tau)$ is called the wavelet coefficient at time t and scale τ, hereafter denoted $\delta_\tau^W \Psi(t)$; it corresponds to a "smoothed" measure of the variations of Ψ at scale τ, denoted $\delta_\tau \Psi = \Psi(t+\tau) - \Psi(t)$. The wavelet transform analysis was performed using the LastWave free software (17), and the convolution was performed using the fast Fourier transform method.

Please cite this article in press as: Lemelle et al., Tumble Kinematics of *Escherichia coli* near a Solid Surface, Biophysical Journal (2020), https://doi.org/10.1016/j.bpj.2020.03.024

A property of such a WT using a Gaussian kernel is that it preserves the scale-invariance properties of the analyzed process: assuming $\Psi(t)$ to be a standard Brownian rotational diffusion process (see Appendix), the probability density function $\rho_\tau(\delta_\tau\Psi(t))$ of the fluctuation variations $\delta_\tau\Psi(t)$ are scale invariant in the statistical sense that they satisfy Eq. 15 (Appendix), with the consequence that the graphs of the rescaled pdf $\tau^{0.5}\rho_\tau(\tau^{0.5}\delta_1\Psi)$ vs. $\delta_1\Psi$ collapse on a single Gaussian curve.

It can be shown (19) that the same relationship holds also for the corresponding wavelet coefficient: the rescaled pdf $\tilde{\rho} = acs(\tau^{0.5}\delta_1^W\Psi)$ vs. $\delta_1^W\Psi$ also collapses on a single Gaussian curve in the Brownian diffusion regime.

RESULTS

A common feature of all tumble events, irrespective of their effect on the trajectory orientation, is a drop in velocity lasting a fraction of a second. Such drops were first spotted in the bulk 3D motion (1). In this study, we also found them in the two-dimensional (2D) motion above solid surfaces. At coarse-grained scale (smoothing at the 100-ms scale), 52 tumbles were detected in speed signals, not as drops in speed but rather as long low-speed events starting (or finishing, respectively) with an abrupt deceleration (or acceleration, respectively) (see Sorting Tumbles). Considering that tumble events initiate with a sharp drop of the speed value, the start of tumbles was indeed defined as the time point with a high value of local velocity drop variations, which corresponds to the high value of the second derivative of the speed. Note that an additional set of 19 events was detected at the end of the trajectories. They were not retained because they were followed by an escape toward the volume. The reorientations resulting from the retained tumbles were then examined at a coarse-grained scale. Although all reorientations were found to coincide with a drop (see Fig. 2 *A* as an example), we found drops without overall reorientation, the final orientation happening to coincide with the initial one after a period of erratic variations (see Fig. 2 *B* as an example). Furthermore, the reorientation fluctuations within the tumbles were analyzed down to a fine-grained scale.

Coarse-grained scale examination of tumbles

Tumbles defined as a drop in speed in swimming trajectories

We first determined characteristic times describing the coarse-grained evolution of speed and orientation in the tumbles (see Sorting Tumbles). These times are relative to the start of the tumble (Fig. 2, *A* and *B*) for all considered events ($N = 52$). We report their mean and standard deviation values in Fig. 2 *C* and their distribution in Fig. S1.

Speed (Fig. 2 *C*) decays over 142 ms ($\langle\tau_2^V\rangle = 142 \pm 33$ ms, N = 52), at an average rate of 75 ± 30 μm s^{-2}. The decrease in speed is of varied amplitude (50 ± 20%). The swimming speed is fully recovered ($\langle V(t_1^V)/V(t_3^V)\rangle \sim 100 \pm 25\%$, $N = 52$) in nearly 325 ms ($\langle\tau_3^V\rangle = 325 \pm 98$ ms, N = 52). The average overestimations of τ_2^V and τ_3^V due to speed smoothing by a window of 114 ms compared with 50 ms were estimated as equal to 8 and 16 ms, respectively (see "Materials and Methods"), and thus almost negligible compared with the variance reported here within the bacterial population.

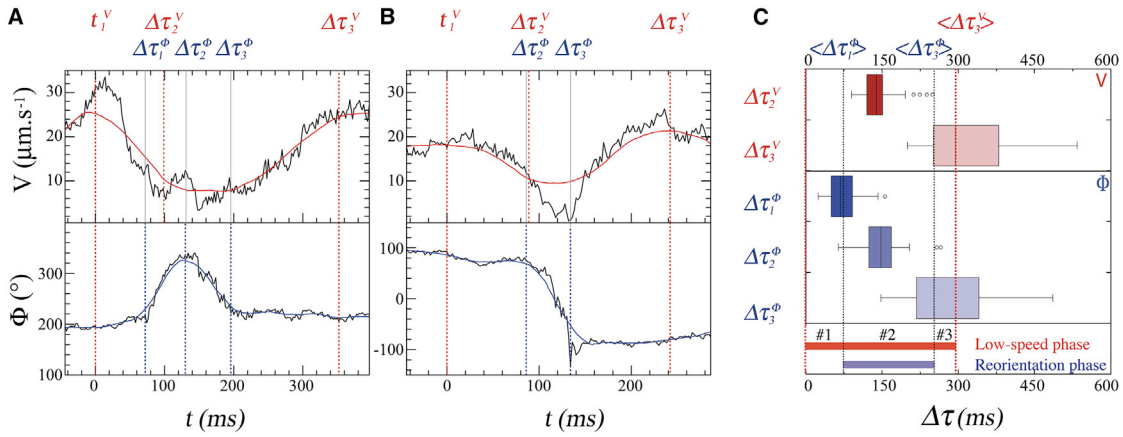

FIGURE 2 Three phases during a tumble near a solid surface. (*A*) A tumble with low reorientation is shown. The speed, *V*, and the direction of the motion, *Φ* (*black lines*), are reported from the start of the "tumble," t_1^V (*common dashed red vertical lines*). The end of the decrease of speed (τ_2^V) and of the "low-speed" phase, τ_3^V, are reported (*dashed red lines*), as well as the speed values smoothed at $L = 114$ ms (*red lines*). The angular reorientation of the trajectory is a phase that starts, reaches a maximal value, and ends at τ_1^Φ, τ_2^Φ, and τ_3^Φ, respectively (*dashed blue lines*), as well as the *Φ*-values smoothed at $L = 50$ ms (*blue lines*). (*B*) A tumble with large reorientation is shown. (*B*) shares the same legend as in (*A*). (*C*) Box plots of the elapsed times τ_2^V (142 ± 33 ms) and of τ_3^V (325 ± 98 ms) are reported for all the tumbles ($N = 52$) in red. Box plots of the elapsed times τ_1^Φ (72 ± 32 ms), τ_2^Φ (147 ± 42 ms), and τ_3^Φ (276 ± 86 ms) for the efficient tumbles ($N = 28$) are reported in blue. The centerlines show the median, and the edges show the first and third quartiles. "Whiskers" extend to the largest and smallest data points within 1.5 interquartile ranges of the first and third quartile. The schema below summarizes the relative positioning of the low-speed phase (in *red*) and the reorientation phase (in *blue*) from which the three phases can be defined: a deceleration phase with no reorientation (*#1*), a reorientation phase (*#2*), and an acceleration with no reorientation (*#3*). To see this figure in color, go online.

Please cite this article in press as: Lemelle et al., Tumble Kinematics of *Escherichia coli* near a Solid Surface, Biophysical Journal (2020), https://doi.org/10.1016/j.bpj.2020.03.024

Trajectory reorientations associated with tumbles

The direction change over the duration $\tau_3^V = t_3^V - t_1^V$ of a tumble is written as

$$\Delta\Phi\left(\tau_3^V\right) = \Phi\left(t_3^V\right) - \Phi\left(t_1^V\right), \tag{9}$$

with Φ defined in Eq. 3. The stochastic component of the direction changes according to

$$\Delta\Psi(\tau) = \Delta\Phi(\tau) - \tau\dot{\Phi}^{mod}, \tag{10}$$

where $\tau = t - t_1^V$ is the elapsed time within the tumble, $\tau\dot{\Phi}^{mod}$ is the deterministic component due to the continuing action of the propulsion during the tumble, and $\dot{\Phi}^{mod}$ is the modal angular velocity computed in the two adjacent surface runs. The overall direction change is then written as

$$\Delta\Psi\left(\tau_3^V\right) = \Delta\Phi\left(\tau_3^V\right) - \tau_3^V\dot{\Phi}^{mod}. \tag{11}$$

Consider the overall change of direction $\Delta\Phi(\tau_3^V) = \Phi(t_3^V) - \Phi(t_1^V)$, defined as the change in trajectory orientation angle between $\Phi(t_1^V)$ at the beginning of the tumble and $\Phi(t_3^V)$ at the end of the tumble observed at a coarse-grained scale (Fig. 2, *A* and *B*, *bottom*).

The distribution of $\Delta\Phi(\tau_3^V)$ shows that the clockwise (CW) reorientation (Fig. 3 *A*) is more frequent (~70%) than the counterclockwise (CCW) reorientation (CW (or CCW, respectively) with angles being positive (or negative, respectively) when viewed from above the surface). The average and dispersion values of $\Delta\Phi(\tau_3^V)$ are 17 ± 70°.

The steady CW curvature due to propulsion near a surface would, if acting during a tumble, reorient the trajectory by $\tau_3^V\dot{\Phi}^{mod}$, where $\dot{\Phi}^{mod}$ is the modal curvature in the adjacent runs. Subtracting this bias, we consider the reorientation angle $\Delta\Psi(\tau_3^V) = \Delta\Phi(\tau_3^V) - \tau_3^V\dot{\Phi}^{mod}$, whose distribution is found to be symmetric and centered on 0.5 ± 77° (Fig. 3 *B*). This supports the idea that, as in the bulk, the propulsion prevailing during the surface runs is still active during tumbles and that it adds to a zero-mean random change.

Near the surface, the distribution of the absolute value $\left|\Delta\Psi(\tau_3^V)\right|$ (Fig. 3 *C*) has a mean value of 52 ± 30°, slightly lower than in the bulk motion, 68 ± 36° (1), with a higher occurrence of large reorientation angle (Fig. 3 *C*).

Reorientation occurs after the initial tumble's deceleration

The variations of the direction angle Φ (Eq. 3) within the tumbles were investigated in the same way as for V: by computing the local extrema of the second time derivative $\ddot{\Phi}$ (time derivatives being taken after smoothing at scale L = 50 ms) and three characteristic times defined in the same way as for $V(t)$. The times elapsed between the initial deceleration time t_1^V and the beginning and the maximum and the end of the trajectory reorientation are denoted $\tau_1^\Phi(=t_1^\Phi - t_1^V)$, $\tau_2^\Phi(=t_2^\Phi - t_1^V)$, and $\tau_3^\Phi(=t_3^\Phi - t_1^V)$, respectively. Unexpectedly, the sharp variations of orientation allowed for the pinpointing of times t_2^Φ and t_3^Φ in only about half of the tumbles (see Fig. S1); the overall orientation $\Delta\Phi(t_3^V)$ being, of course, available in all observed tumbles (N = 52). In these cases, the reorientation of the trajectory (Fig. 2 *C*) started midway along the drop in speed (τ_1^Φ in Fig. 2 *C*) and increased as the speed decreased until both reached their extrema almost simultaneously (at τ_2^Φ and at τ_2^V in Fig. 2 *C*). The final orientation was reached within time $\tau_3^\Phi = t_3^\Phi - t_1^V$ = 276 ± 86 ms (N = 45) before speed was fully recovered.

This coarse-grained study displays a three-phase sequence of the progress of a tumble. An abrupt speed deceleration phase first occurs in the direction of the preceding run. It is followed by a reorientation phase of the trajectory that starts abruptly. In all cases, it ends with an abrupt speed acceleration phase in the direction of the next run (Fig. 2 *C*). The full sequence is shown here to be much longer (325 ± 98 ms, N = 52) than the reorientation phase (176 ± 79 ms). The values of deceleration and acceleration mean durations are more comparable than to be expected from first reports (1). The distribution of the reorientation angles due to tumbles is symmetric and centered on 0.5 ± 77° (Fig. 3 *B*) and indicates a forward persistence of the *E. coli* motion slightly higher than in the bulk. Unlike that observed in the bulk, the most probable reorientation is

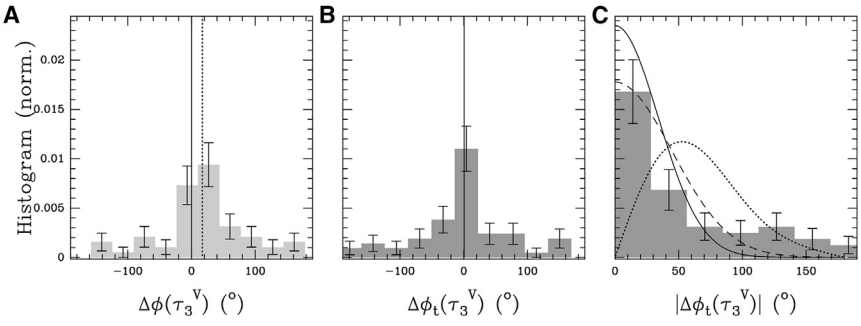

FIGURE 3 Distributions of the change in direction after a tumble. (*A*) Normalized distribution of the reorientation angles $\Delta\Phi(\tau_3^V)$ of the 52 tumbles (bin size 36°) (*light gray bars*) is shown. Positive angles turn CW. The mean value (*vertical dotted line*) and dispersion are 17 ± 70°. (*B*) The normalized distribution of the centered reorientation angle $\Delta\Psi(\tau_3^V) = \Delta\Phi(\tau_3^V) - \tau_3^V\Phi^{mod}$ (*gray bars*) is shown. (*C*) Bulk distribution of the reorientation angle first measured by Berg and Brown (1) (*black dotted line*, D = 3.5 rad^2/s) versus the corresponding surface distribution (*black dashed curve*) is shown. Normalized distribution of the absolute value of the near-surface reorientation angle $\left|\Delta\Psi(\tau_3^V)\right|$ (*gray bars*) and the theoretical distribution (Eq. 15, *black curve*) calculated as a diffusive process (D = 1 rad^2/s) considering an average reorientation time $\langle\tau_3^V\rangle$ is shown.

Please cite this article in press as: Lemelle et al., Tumble Kinematics of *Escherichia coli* near a Solid Surface, Biophysical Journal (2020), https://doi.org/10.1016/j.bpj.2020.03.024

actually zero, and there is a higher occurrence of large reorientation angles (Fig. 3 *C*). These observations made at the coarse-grained scale within tumbles were thoroughly examined by a multiscale analysis.

Multiscale analysis of orientation fluctuations within tumbles

Two regimes of orientation fluctuation

The Ψ-value fluctuations, $\delta\Psi$, were investigated through a multiscale analysis within the wavelet transform framework, with the first derivative of the Gaussian as the mother wavelet (Eq. 8; (20)) (see Wavelet Analysis of the Direction Fluctuations in Materials and Methods). We chose to analyze Ψ rather than Φ (Eq. 10) to eliminate the systematic curvature bias due to propulsion.

The values of the local fluctuations $\left|\delta_\tau^W \Psi(t)\right|$, i.e., the wavelet coefficients (see Materials and Methods), obtained at every instance of an event, (t) (x axis) and for different timescales, τ, ranging from 4 to 55 ms (y axis in 2-base log), are reported as a heatmap for each tumble. As shown in Figs. 4 *A* and S4–S13, the events of large reorientation are observable at all timescales within a tumble. They are short-term and large reorientation events that seem to arise sporadically. They are called "bursts."

The distributions of all the fluctuation values measured within all the tumbles at different τ-scales, once rescaled, $\tilde{\rho}_\tau$ (see Materials and Methods) are reported in Fig. 4 *B*. The applied rescaling (i.e., $1/\tau^{0.5}$) enables the display of diffusion fluctuations along a Gaussian distribution and, finally, to evaluate a corresponding diffusivity value (see Eq. 15 in Appendix). Indeed, for a standard orientational diffusion process, fluctuations of the orientation at all timescales $\delta_\tau\Psi$ are normally distributed, with variance $\sigma_\tau^2 = \sigma_1^2\tau$ and $D = \sigma_1/2$ (see Appendix). Here, the distribution reveals two regimes:

1. a small fluctuations regime that rescales as a Gaussian diffusive process ($\delta_1^W\Psi/\tau^{0.5}$ within the *dashed lines* in Fig. 4 *B*) or
2. a noncanonical statistics regime with a large heavy tail ($\delta_1^W\Psi$ outside the *dotted lines* in Fig. 4 *B*).

The bursts

The burst detection uses the fact that the corresponding $\delta_\tau^W\Psi$ fluctuations must not follow the canonical diffusive $1/\tau^{0.5}$ timescale rescaling of Eq. 16, characterized by a direction diffusivity value of a few $rad^2\ s^{-1}$ (21). An apparent diffusivity value was evaluated for each tumble from Eq. 14 and the fluctuation values at the 6-ms scale (Fig. 5 *A*). Two sets of reorientations of about the same number were separated by a threshold value just above 2 $rad^2\ s^{-1}$, corresponding to a 1σ of the probability density distribution (see Eq. 12) value of 3.8°. A burst event was then detected within a tumble as a fluctuation higher than the 3σ-value ($\left|\delta_\tau^W\Psi/\tau^{0.5}\right| > 11.4°$, $\tau = 6$ ms; see Fig. 5 *B*). Conversely, a lower fluctuation was regarded as belonging to a nonburst event. No burst was detected within 25 of the 52 selected tumbles, and at least one burst was detected in the 27 remaining tumbles, with a major impact on the corresponding calculated diffusivity values shown in Fig. 5 *A*. Considering that contiguous instants (separated by less than one frame) of the detected fluctuations are related to a unique event of "burst of reorientation," 89 bursts were identified in 27 tumbles.

The beginning and the end of bursts #I were denoted as $t_{1,i}^\Psi$ and $t_{3,i}^\Psi$, respectively; the duration of the burst, $\tau_{burst,i} = t_{3,i}^\Psi - t_{1,i}^\Psi$; and the elapsed time until the next burst (if any), $\tau_{interburst,i} = t_{1,i+1}^\Psi - t_{3,i}^\Psi$. The elapsed time before the first burst, $\tau_{1,1}^\Psi = t_{1,1}^\Psi - t_1^V$, and after the last burst, denoted $\tau_{1,*}^\Psi = t_3^V - t_{1,l}^\Psi$, were sorted to specify the sequence

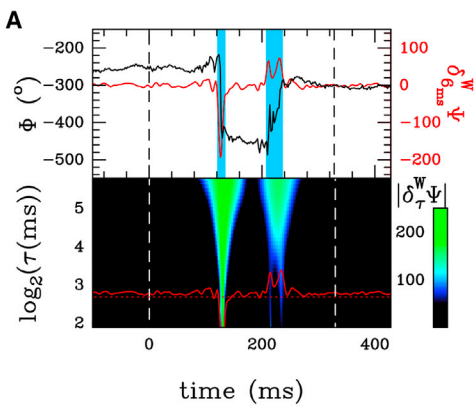

FIGURE 4 Wavelet transform analysis of orientation fluctuations. (*A*, *top*) The orientation angle Φ (*black line*, *left axis*) reported for one tumble is shown. The red curve (on the *right axis*) corresponds to the variations of Ψ as measured at scale 6 ms ($\delta_\tau^W\Phi(t)$) reported for one tumble. The start and the end of the tumble are marked by a dashed vertical line. Abrupt reorientation events occur in regions highlighted by blue boxes, which form two sets of bursts of reorientation. (*A*, *bottom*) Heatmap of the wavelet coefficient $\delta_\tau^W\Psi(t)$ at time t (x axis) and scale τ (y axis in 2-base log), provided by the analysis of the $\Phi(t)$ profile reported in the top panel, is shown. The red curve is also reported. (*B*) Rescaled probability density function $\ln(\tilde{\rho}) = \ln(\tau^{1/2}\rho_\tau(\tau^{0.5}\delta_1^W\Psi))$ vs. $\delta_1^W\Psi$ for a set of scales ranging from 4 ms (*black circles*) to 55 ms (*red circles*) when the analysis was performed on all the duration $\Phi(t)$ profiles of all the tumbles. The vertical dashed lines delimitate a small fluctuations regime that rescales as a Gaussian diffusive process ($\delta_1^W\Psi/\tau^{0.5} < 7.6°$; see main text for the value), and the dotted lines delimitate the noncanonical statistics regime with a large heavy tail, respectively ($\left|\delta_1^W\Psi\right| > 11.4°$|; see main text for the value). The Gaussian distribution of $\delta_{1ms}^W\Phi$ of a diffusive process characterized by $D = 1.5\ rad^2 \cdot s^{-1}$ (*black line*) is also reported. To see this figure in color, go online.

Please cite this article in press as: Lemelle et al., Tumble Kinematics of *Escherichia coli* near a Solid Surface, Biophysical Journal (2020), https://doi.org/10.1016/j.bpj.2020.03.024

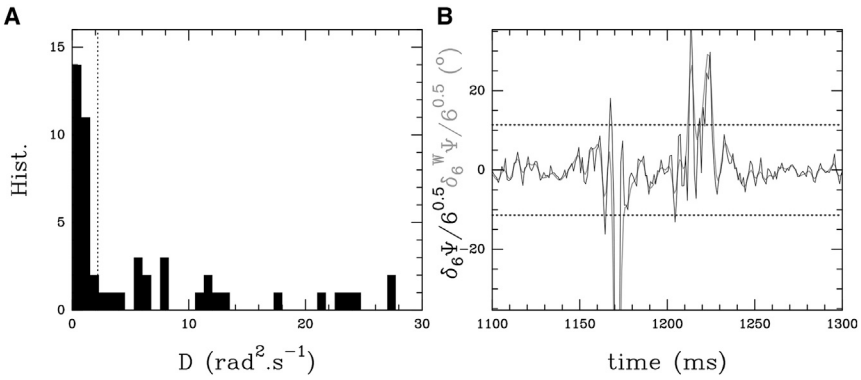

FIGURE 5 Detection of the bursts. (*A*) The distribution of the apparent D-values of the 52 tumbles is shown. Each apparent D-value was compiled from Eq. 14 (Appendix) and the fluctuations values observed at the 6-ms scale within a tumble. We used an arbitrary threshold value of 2.2 rad^2/s to split the population into two sets and verified a posteriori that bursts were detected only in the set of high apparent D values. The 1σ-value of the probability density distribution (see Eq. 12) corresponding to the 2.2 rad^2/s diffusivity is 3.8°. (*B*) The comparison of the Φ variations within a tumble reported for every instance is shown, once smoothed with a sliding window of three frames (*black line*) or computed in the wavelets framework of this study at scale 6 ms ($\delta_{6\ ms}^{g^{(1)}}\Phi(t)$ (*gray line*). The fluctuation values at 3σ from zero ($\left|\delta_{6ms}^{W}\Psi/\tau^{0.5}\right| = 11.4°$) are reported (*horizontal dotted lines*). Bursts were defined as events of contiguous fluctuations that fall away from the 3σ-values.

of the progress of the tumble progress. The reorientations due to bursts #*I*, $\Delta\Psi_{burst,i} = \Psi_{3,i} - \Psi_{1,i}$, were measured.

A burst is typically a very short event, with a duration τ_{burst} lasting 10.6 ± 6.4 ms (Fig. 6 *A*). A small average number of bursts (3.3 ± 2) were detected within a tumble with a burst. The first burst starts 120 ± 30 ms after the beginning of the tumble and 112 ± 54 ms before the end of the tumble (Fig. 6 *B*), bracketing a period of ~100 ms. The elapsed time between two consecutive bursts, $\tau_{interburst}$, can be either comparable to the burst duration or be much longer, with interburst values ranging from 20 to 100 ms (Fig. 6 *A*). So, bursts occur at a high rate (10 ms) just before and after the 100-ms period they bracket. They are events concentrating drastic absolute angular reorientations, $|\Delta\Phi_{burst}|$ (69.6 ± 66°, $N = 89$) (Fig. 6 *C*). They occur almost equally in a single CW or CCW direction, so the corresponding average angular reorientation, $\Delta\Phi_{burst}$, is 12 ± 89.9°.

The directional diffusion outside of the bursts

In the small fluctuations regime, two phenomena can be distinguished within the tumbles. One is mainly observed near the surface runs (Fig. S2 *A*) and less frequently within the tumbles (Fig. S2 *B*). This can be accounted for by a diffusion process in which the diffusivity value is of ~0.3 rad^2 s^{-1}. The other one, of intermediate amplitude, prevails within tumbles and can be accounted for by a diffusion process in which the diffusivity value is of ~1.5 rad^2/s (Fig. S2 *B*). Such diffusivity can also be evidenced by computing the directional autocorrelation function $\langle\cos\delta_\tau\Phi\rangle$ within every tumble (see Appendix). For a standard Gaussian diffusion process, it decreases exponentially $\langle\cos\delta_\tau\Phi\rangle = \exp -2D\tau$ (see Appendix), with D the diffusion constant. As shown in Fig. S3, there is a clear distinction between the two sets of tumbling, without and with bursts. As expected, the first set without bursts shows decreasing autocorrelation functions with a surface diffusivity value

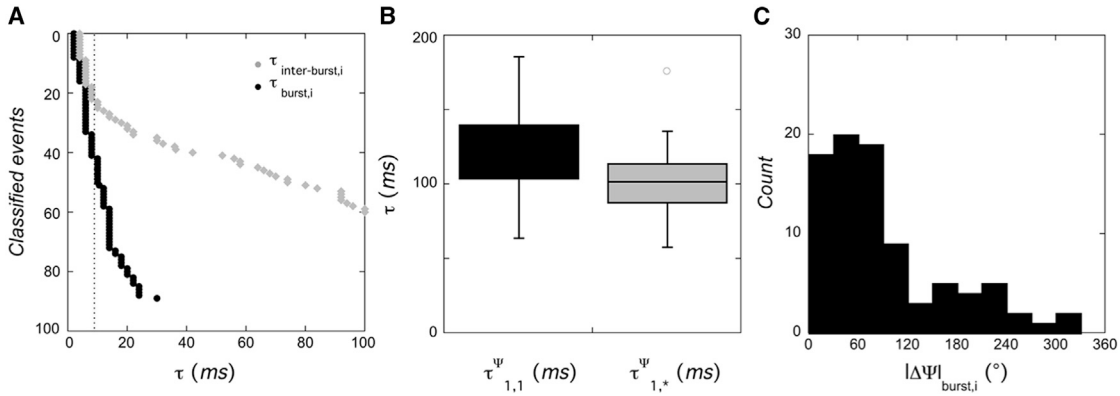

FIGURE 6 The properties of the 89 detected bursts. (*A*) The duration of a burst, τ_{burst} ($N = 89$, *black solid circles*), and the elapsed time between two consecutive bursts, $\tau_{interburst}$ ($N = 62$, *gray solid circles*), are shown. They were both sorted vertically. The vertical dashed line delimitates a value below which the elapsed time between two consecutive bursts, $\tau_{interburst}$, is comparable to the burst duration. (*B*) Box plots of the elapsed time within the tumble before the first burst, $\tau^{\Phi}_{1,1}$, and after the last burst, $\tau^{\Phi}_{1,*}$, for the 27 tumbles displaying bursts are shown. The centerlines show the median, and the edges show the first and third quartiles. "Whiskers" extend to the largest and smallest data points within 1.5 interquartile ranges of the first and third quartile. (*C*) The distribution of the absolute angular reorientations after a burst, $\Delta\Psi_{burst}$, is shown.

Please cite this article in press as: Lemelle et al., Tumble Kinematics of *Escherichia coli* near a Solid Surface, Biophysical Journal (2020), https://doi.org/10.1016/j.bpj.2020.03.024

close to 1.5 rad^2/s. In contrast, the second set (with bursts) cannot be approximated by exponentially decreasing autocorrelation functions, confirming the nonstandard nature (i.e., Gaussian diffusion) of stochastic reorientation via the discrete bursts.

Tumbles near solid surfaces are, as in the bulk, diffusive events of diffusivity values 10 times higher than in the surface runs, on top of which bursts of reorientation destabilize the cell-swimming direction in half of the cases. The persistence of the motion results in drastically different "with" or "without" bursts.

DISCUSSION

The compliance of the set of tumbles with the founding description of the bulk run-and-tumble motion (1) was preliminarily verified. The selected 52 events, with or without the 19 terminal deceleration events, and the total 58-s duration of the selected trajectories point to a tumbling rate value of ~1 Hz in accordance with the bulk tumbling frequency value. Speed is also transiently lowered, and bacteria fully recover their surface swimming speed at the end of the tumbles (~100 ± 25%, $N = 52$). Similarly, tumbles are associated with a symmetric reorientation distribution that centers around zero (once the CW surface propulsion of the bacterium is subtracted), which supports the idea that the propulsion prevailing during the surface runs is still active during surface tumbles, as in the bulk (3). However, the differentiation of the two types of tumble is specifically related to the presence of the surface. The surface-flagella interaction is discussed below as the most probable mechanism underlying the differentiation.

Tumbles near solid surfaces without bursts were shown to be diffusive events with higher diffusivity than in the surface runs (values up to five times higher), as in the bulk (values up to 10 times higher), but with a much stronger direction persistence ($\langle \cos \Delta\Phi_t \rangle > 0.8$) than in the bulk (~0.66). Following Saragosti et al. (18), which describes tumbles in the bulk by a 3D rotational diffusion of the bacteria body, we can describe tumbles near a solid surface by the same stochastic process with the additional constraint of 2D confinement as developed in Eq. 12 of Appendix. The average diffusivity values evaluated from the orientation fluctuations within the tumbles and the average directional autocorrelation functions are ~1.5 and 1 rad^2/s, though very comparable to the values reported for tumbles in the bulk (2,18). Interestingly, such a model predicts the much stronger directional persistence ($\langle \cos \Delta\Phi_t \rangle > 0.8$) near a solid surface than in the bulk (~0.66). So, these tumbles can be considered as classical tumbles. Their progress must, therefore, bring into play the same flagellar conformational transitions than in a bulk tumble and also some specific process resulting in a 2D confinement that occurs specifically in the surface proximity. These tumbles are said to be 2D confined (annotated T_c).

Tumbles near solid surfaces with bursts were shown to be diffusive events similar to tumbles without bursts, on top of which bursts of reorientation destabilize the cell-swimming direction. They are characterized by a low persistence related to the presence of bursts. The partial anticorrelation displayed by the directional autocorrelation functions at 100 ms and an almost full randomization ($\langle \cos \delta\Phi_t \rangle = 0$) at $\tau = 200$ ms cannot be accounted for by a unique rotational diffusion process throughout the entire period of the tumble. The low persistence of these tumbles implies a nondiffusing process that enhances reorientation, specifically in the surface proximity. These tumbles are said to be exacerbated (annotated T_e).

Whether bacteria are prone to the T_c or T_e type brings some constraint to the tumble mechanisms near the surface. Among the 25 exacerbated tumbles and the 27 2D-confined tumbles, there were 3, 8, 4, and 5 $T_e \rightarrow T_e$-, $T_e \rightarrow T_c$-, $T_c \rightarrow T_e$-, and $T_c \rightarrow T_c$-paired tumbles, respectively; so, bacteria can alternate between the two types of tumble. Should the T_e and T_c tumbles occur independently with occurrences of $f_e = 48\%$ and $f_c = 52\%$, the expected number of pairs would be 4.6, 5, 5, and 5.4, respectively. The divergence between the observed and expected distributions is measured by $\chi^2 = 2.6$, with a corresponding p-value of 0.46, indicating that the hypothesis of independence is compatible with the observations. Any bacterium swimming near and parallel to a solid surface performs exacerbated and 2D-confined tumbles with roughly the same probability. As a consequence, bursts of reorientation that prompt about half the time T_e over T_c tumbles near a surface must be triggered by a mechanism common to all the swimming bacteria, the flagellar mechanism involved in a tumble (3).

The three-stage sequence of the tumbles with bursts strengthens the hypothesis of a tumble progress driven by the same flagella-conformational transitions as in the bulk and of their crucial role in the surface differentiation of two types of tumble. In this sequence, an abrupt speed deceleration phase occurs in the direction of the preceding surface run, lasting ~100 ms. It is followed by a reorientation phase displaying a typical tumbling diffusivity value and burst positioned preferentially at the beginning and the end of this period. It is ended by a symmetric increase in speed (as abrupt and of similar length), which was difficult to predict from previous speed increase observations (1). This three-stage sequence was shown to be also valid within every individual event (Fig. S1). The mechanisms underlying progression of the tumble must be controlled at the single-cell scale, as is the flagellar mechanism involved in tumbles (3).

The order of this three-stage sequence with the six-stage sequence (4) of the flagella conformations within a tumble (3,4) brings, besides pinpointing characteristic times on the model of flagella conformation, a focus on the specific flagellar conformations possibly involved in the surface differentiation of the two types of tumble. The end of a run

Please cite this article in press as: Lemelle et al., Tumble Kinematics of *Escherichia coli* near a Solid Surface, Biophysical Journal (2020), https://doi.org/10.1016/j.bpj.2020.03.024

(*stage annotated #1* in Fig. 7 as in (4)) must indeed be triggered by the initial reversal (CCW to CW) of one motor driving one individual flagellar filament coalesced in a bundle. The consecutive phase of speed decay with no reorientation suggests that the flagellar configuration is most probably that of a bundle with a decreased propulsion efficiency caused by the left-handed flagellum rotating in the opposite direction to the bundle (*#2* in Fig. 7). Conversely, the speed increase with no reorientation of the "ending propulsion phase" must be triggered by the switch of the motor (CW to CCW) causing the right-handed flagellum loosely twisted around the bundle to revert to its normal form within the bundle (*#7* in Fig. 7). The reversal completion initiates the next run (*#8* in Fig. 7) and the full recovery of the bundle efficiency. So, the flagellar conformations immediately after or preceding the flawed bundles must be those accounting for the two types of tumble.

The dynamics of the few-micrometers-long flagellar filaments, partly thrown out from the bundle during the reorientation of the bacterial body in the bulk, were expected to be influenced by the close proximity of a solid surface (within 2 μm in this study). The comparable and uncorrelated probability of occurrence of the two types of reorientation leads us to relate them to the release either toward the surface or toward the bulk of the flagellum out of the bundle that actuates the reorientation (right semi-coiled filament). If released in the bulk, a steric surface hindering of the angular diffusivity perpendicular to the surface of the bacterium, as observed during the propulsion (13), could account for the observed 2D confinement parallel to the surface. If released toward the surface, steric interactions with this particular flagellum may induce short-term and large reorientation (22). The two average values for the duration between two consecutive bursts of ~10 ms (100 Hz) and 80 ms (12.5 Hz) may be interpreted by two types of repetitive contact of the flagellum with the surface: those due to the flagellar rotation (at ~100 Hz) and those due to the full rotation of the body (at ~12.5 Hz). Direct observations with microscopes that couple simultaneous observations of the flagella and body motions (23) are crucial to attest to the flagellar mechanism proposed in this study.

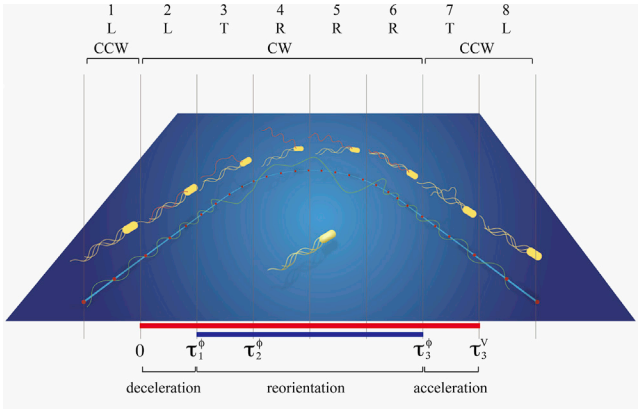

FIGURE 7 Model sequence of the body motion during a tumble. This figure was constructed based on that of Darnton et al. (4), which sums up the observations of the polymorphic transformations of the flagella and their interpretation in terms of reorientation of the motion within a canonical tumble caused by the reversal of a single motor. The upper timeline indicates the direction of motor rotation of the filament causing the tumble (*CW rotation* in *red*, *CCW rotation* in *yellow*). L is annotated when the filament is left-handed, R is annotated when the filament is right-handed, and T is annotated for transitions. The different body motions deduced from the speed, V, the direction of the motion, Φ, and the body orientation relative to the trajectory, θ, analyzes are superimposed on this schema. The speed is rendered graphically by the length between consecutive red dots representing the centroids of the image of the body projected onto the surface that are sampled at a constant frequency. The motion direction is indicated by the blue line passing through the red dots. For the sake of simplicity, the CW circular trajectory in the run phases is represented with a very low curvature value. The below the drawing, shows the relative positioning of the low-speed phase (in *red*) and the reorientation phase (in *blue*) together with the main characteristic times (τ_1^Φ, τ_2^Φ, τ_3^Φ, and τ_3^V). This highlights the three-phase sequence: a deceleration phase with no reorientation, a reorientation phase, and an acceleration phase with no reorientation. To see this figure in color, go online.

Intuitively, it is expected that both the circular motion and the nonslipping interface hinder the diffusion of the bacteria away from a solid surface and therefore favor adhesion to the surface to form a biofilm. However, this study shows that a surface can be a source of significant reorientation via the bursts and thereby allows the dissemination or escape of bacteria from the surface. The series of tumbles, alternating more persistent and large reorientation events than in bulk (24), let us expect a specific superdiffusive behavior close to surface. Bacteria may have a specific chemotaxis response different on the surface from that in the bulk.

CONCLUSION

We report bacteria reorientation close to a surface due to tumbling with an equiprobable change in direction (CW, CCW). That reorientation is superimposed on a CW path because of persistent propulsion. The first half of the tumbles are accounted for by an active rotational diffusion of the bacterial body confined parallel to the surface with a diffusivity value of (1.5 rad^2/s) comparable to that measured in the bulk. The second half of a tumble is highly efficient. The reorientation phase is much shorter than the low-speed phase, and the reorientation is accounted for by few-millisecond bursts of almost equiprobable CW or CCW change of direction ($70 \pm 66°$, $N = 89$) that destabilize the cell-swimming direction. They are most probably sustained by the contact of the flagellum released from the bundle with the surface. These observations of surface tumbles provide evidence to further investigate the cell-surface mechanism by a direct report of flagella dynamics near a solid surface. Transient adhesion on the surface has been proposed as a mechanism to regulate the surface exploration by *E. coli*

Please cite this article in press as: Lemelle et al., Tumble Kinematics of *Escherichia coli* near a Solid Surface, Biophysical Journal (2020), https://doi.org/10.1016/j.bpj.2020.03.024

(25). This study shows that surface tumbles are also involved in the optimization of the surface exploration and that swimming bacteria may develop some specific chemotaxis faculties near solid surfaces.

APPENDIX: THE TUMBLE PROCESS AS A 2D-ROTATIONAL BROWNIAN DIFFUSION

Following Saragosti et al. (18), if we assume that the reorientation during tumble obeys the same stochastic process as in three dimensions (bulk), but with an additional constraint of 2D confinement, the orientation of the motion is defined by a unique angle Φ that obeys the following 2D-rotational Brownian diffusion equation:

$$\frac{\partial p}{\partial t} = D\frac{\partial^2 p}{\partial \Phi^2}, \tag{12}$$

where p is the probability density distribution to have an orientation Φ at a given time t and D is the rotational diffusion constant. The statistical distribution of the reorientation occurring within time τ, $\delta_\tau\Phi(t) = \Phi(t+\tau) - \Phi(t)$, $t > 0$ is given by the following equation:

$$p(\delta_\tau\Phi) = \frac{1}{\sqrt{4\pi D\tau}} e^{-(\delta\Phi)^2/(4D\tau)}. \tag{13}$$

Consequently, the reorientation fluctuations and the directional autocorrelation function after time τ obey the following relations:

$$\langle \delta\Phi \rangle = 0, \tag{14}$$

$$\left\langle (\delta_\tau\Phi)^2 \right\rangle = 2D\tau, \tag{15}$$

$$\langle \cos\delta_\tau\Phi \rangle = e^{-D\tau}, \tag{16}$$

$$\langle \sin\delta_\tau\Phi \rangle = 0, \tag{17}$$

Such a Gaussian diffusion process belongs to the class of self-similar stochastic process with scale-invariant statistics of variations fluctuations; indeed, we directly derive from Eq. 13 that $\tau^{0.5}\rho_\tau(\tau^{0.5}\delta\Phi) = \rho_1(\delta\Phi)$, where $\rho_1(\delta\Phi) = \mathcal{N}(0, \sigma_1^2 = 2D)$ is the distribution of reorientation fluctuation at the unit timescale.

The 2D-rotational diffusion is twice-more persistent than the 3D diffusion assuming a same diffusion constant (in three dimensions, $\langle \cos\Delta\Phi(\tau) \rangle = e^{-2D\tau}$). The typical reorientation $\Delta\Phi_t$ during a tumble phase, assuming again an exponentially distributed tumble duration time of mean value τ_t, is therefore given by the following equation:

$$\Delta\Phi(\tau_t) \sim \mathcal{N}(0, 2D\tau_t) = \frac{1}{\sqrt{4\pi D\tau_t}} e^{-(\Delta\Phi)^2/(4D\tau_t)}. \tag{18}$$

Let us note here that this distribution can only account for an unbiased reorientation process (i.e., of zero mean) and, in particular, has to be compared with the "centered/unbiased" experimental reorientation angles $\Delta\Psi(\tau_t) = \Delta\Phi(\tau_t) - \tau_t\dot{\Phi}^{mod}$, where $\tau_t\dot{\Phi}^{mod}$ corresponds to the deterministic reorientation part because of the circular propulsion that remains during tumbling (see text).

For bacteria swimming near a surface, there is indeed reorientation contribution from the propulsion, leading to a diffusion-convection process whereby Φ undergoes, in addition to the diffusive process just described, a constant drift at the rate $\dot{\Phi}^{mod}$ because of the trajectory curvature. The corresponding angular reorientation distribution is written as

$$p(\delta_\tau\Phi) = \frac{1}{\sqrt{4\pi D\tau}} e^{-\left(\delta\Phi - \dot{\Phi}^{mod}\tau\right)/(4D\tau)}. \tag{19}$$

such that

$$\langle \delta_\tau\Phi \rangle = \dot{\Phi}^{mod}\tau, \tag{20}$$

$$\left\langle (\delta_\tau\Phi)^2 \right\rangle = 2D\tau + \left(\dot{\Phi}^{mod}\tau\right)^2, \tag{21}$$

$$\langle \cos\delta_\tau\Phi \rangle = \cos\left(\dot{\Phi}^{mod}\tau\right) e^{-D\tau}, \tag{22}$$

$$\langle \sin\delta_\tau\Phi \rangle = \sin\left(\dot{\Phi}^{mod}\tau\right) e^{-D\tau}. \tag{23}$$

SUPPORTING MATERIAL

Supporting Material can be found online at https://doi.org/10.1016/j.bpj.2020.03.024.

AUTHOR CONTRIBUTIONS

L.L., C.V., and J.-F.P. developed the concept of the study. L.L., C.P., T.C., A.D., and E.C. performed the experiment. T.C., A.D., and R.B. contributed new imaging tools. C.V. and L.L. conducted the analysis. L.L., C.P., C.V., and J.-F.P. contributed to data interpretation and drafting of the manuscript.

ACKNOWLEDGMENTS

This work was supported by the Agence Nationale de la Recherche (ANR-CONES).

REFERENCES

1. Berg, H. C., and D. A. Brown. 1972. Chemotaxis in *Escherichia coli* analysed by three-dimensional tracking. *Nature*. 239:500–504.
2. Saragosti, J., V. Calvez, …, P. Silberzan. 2011. Directional persistence of chemotactic bacteria in a traveling concentration wave. *Proc. Natl. Acad. Sci. USA*. 108:16235–16240.
3. Turner, L., W. S. Ryu, and H. C. Berg. 2000. Real-time imaging of fluorescent flagellar filaments. *J. Bacteriol.* 182:2793–2801.
4. Darnton, N. C., L. Turner, …, H. C. Berg. 2007. On torque and tumbling in swimming *Escherichia coli*. *J. Bacteriol.* 189:1756–1764.
5. Frymier, P. D., R. M. Ford, …, P. T. Cummings. 1995. Three-dimensional tracking of motile bacteria near a solid planar surface. *Proc. Natl. Acad. Sci. USA*. 92:6195–6199.
6. Lemelle, L., J.-F. Palierne, …, C. Place. 2013. Curvature reversal of the circular motion of swimming bacteria probes for slip at solid/liquid interfaces. *Soft Matter.* 9:9759–9762.
7. Li, G., L. K. Tam, and J. X. Tang. 2008. Amplified effect of Brownian motion in bacterial near-surface swimming. *Proc. Natl. Acad. Sci. USA*. 105:18355–18359.

8. Lauga, E., W. R. DiLuzio, …, H. A. Stone. 2006. Swimming in circles: motion of bacteria near solid boundaries. *Biophys. J.* 90:400–412.
9. Lopez, D., and E. Lauga. 2014. Dynamics of swimming bacteria at complex interfaces. *Phys. Fluids.* 26:071902.
10. Berke, A. P., L. Turner, …, E. Lauga. 2008. Hydrodynamic attraction of swimming microorganisms by surfaces. *Phys. Rev. Lett.* 101:038102.
11. Vigeant, M. A., and R. M. Ford. 1997. Interactions between motile *Escherichia coli* and glass in media with various ionic strengths, as observed with a three-dimensional-tracking microscope. *Appl. Environ. Microbiol.* 63:3474–3479.
12. Drescher, K., J. Dunkel, …, R. E. Goldstein. 2011. Fluid dynamics and noise in bacterial cell-cell and cell-surface scattering. *Proc. Natl. Acad. Sci. USA.* 108:10940–10945.
13. Bianchi, S., F. Saglimbeni, and R. Di Leonardo. 2017. Holographic imaging reveals the mechanism of wall entrament in swimming bacteria. *Phys. Rev. X.* 7:011010.
14. Fahrner, K. A., W. S. Ryu, and H. C. Berg. 2003. Biomechanics: bacterial flagellar switching under load. *Nature.* 423:938.
15. Molaei, M., M. Barry, …, J. Sheng. 2014. Failed escape: solid surfaces prevent tumbling of *Escherichia coli*. *Phys. Rev. Lett.* 113:068103.
16. Son, K., J. S. Guasto, and R. Stocker. 2013. Bacteria can exploit a flagellar buckling instability to change direction. *Nat. Phys.* 9:494–498.
17. Rosser, G., A. G. Fletcher, …, R. E. Baker. 2013. Novel methods for analysing bacterial tracks reveal persistence in *Rhodobacter sphaeroides*. *PLoS Comput. Biol.* 9:e1003276.
18. Saragosti, J., P. Silberzan, and A. Buguin. 2012. Modeling *E. coli* tumbles by rotational diffusion. Implications for chemotaxis. *PLoS One.* 7:e35412.
19. Audit, B., E. Bacry, …, A. Arneodo. 2000. Wavelet-based estimators of scaling behavior. *IEEE Trans. Inf. Theory.* 48:2938–2954.
20. Audit, B., C. Thermes, …, A. Arneodo. 2001. Long-range correlations in genomic DNA: a signature of the nucleosomal structure. *Phys. Rev. Lett.* 86:2471–2474.
21. Fraley, C., and A. E. Raftery. 2002. Model-based clustering, discriminant analysis, and density estimation. *J. Am. Stat. Assoc.* 97:611–631.
22. Kantsler, V., J. Dunkel, …, R. E. Goldstein. 2013. Ciliary contact interactions dominate surface scattering of swimming eukaryotes. *Proc. Natl. Acad. Sci. USA.* 110:1187–1192.
23. Turner, L., L. Ping, …, H. C. Berg. 2016. Visualizing flagella while tracking bacteria. *Biophys. J.* 111:630–639.
24. Kirkegaard, J. B., and R. E. Goldstein. 2018. The role of tumbling frequency and persistence in optimal run-and-tumble chemotaxis. *IMA J. Appl. Math.* 83:700–719.
25. Ipina, E. P., S. Otte, …, F. Peruani. 2019. Bacteria display optimal transport near surfaces. *Nat. Phys.* 15:610–615.